



Wintertime supraglacial lake drainage cascade triggers large-scale ice flow response in Greenland

Maier, Nathan; Andersen, Jonas Kvist; Mouginot, Jérémie; Gimbert, Florent; Gagliardini, Olivier

Published in:
Geophysical Research Letters

Link to article, DOI:
[10.1029/2022GL102251](https://doi.org/10.1029/2022GL102251)

Publication date:
2023

Document Version
Publisher's PDF, also known as Version of record

[Link back to DTU Orbit](#)

Citation (APA):
Maier, N., Andersen, J. K., Mouginot, J., Gimbert, F., & Gagliardini, O. (2023). Wintertime supraglacial lake drainage cascade triggers large-scale ice flow response in Greenland. *Geophysical Research Letters*, 50(4), Article e2022GL102251. <https://doi.org/10.1029/2022GL102251>

General rights

Copyright and moral rights for the publications made accessible in the public portal are retained by the authors and/or other copyright owners and it is a condition of accessing publications that users recognise and abide by the legal requirements associated with these rights.

- Users may download and print one copy of any publication from the public portal for the purpose of private study or research.
- You may not further distribute the material or use it for any profit-making activity or commercial gain
- You may freely distribute the URL identifying the publication in the public portal

If you believe that this document breaches copyright please contact us providing details, and we will remove access to the work immediately and investigate your claim.

Geophysical Research Letters[®]

RESEARCH LETTER

10.1029/2022GL102251

Key Points:

- A cascade of supraglacial lake drainages and an associated ice-flow acceleration are observed during winter in Greenland
- Decomposition of motion into vertical and horizontal components allows for subglacial water pathways and links with sliding to be inferred
- Tracking the history of the supraglacial lakes shows some of the meltwater released was produced decades earlier

Supporting Information:

Supporting Information may be found in the online version of this article.

Correspondence to:

N. Maier,
ntmaier@gmail.com

Citation:

Maier, N., Andersen, J. K., Mouginit, J., Gimbert, F., & Gagliardini, O. (2023). Wintertime supraglacial lake drainage cascade triggers large-scale ice flow response in Greenland. *Geophysical Research Letters*, 50, e2022GL102251. <https://doi.org/10.1029/2022GL102251>

Received 29 NOV 2022

Accepted 18 JAN 2023

Author Contributions:

Conceptualization: Nathan Maier, Jonas Kvist Andersen, Jérémie Mouginit, Florent Gimbert, Olivier Gagliardini

Formal analysis: Nathan Maier, Jonas Kvist Andersen, Jérémie Mouginit

Funding acquisition: Jérémie Mouginit, Florent Gimbert, Olivier Gagliardini

Investigation: Nathan Maier



Visualization: Nathan Maier, Jonas Kvist Andersen, Jérémie Mouginit

Writing – original draft: Nathan Maier, Jonas Kvist Andersen, Jérémie Mouginit, Florent Gimbert

© 2023 The Authors.

This is an open access article under the terms of the [Creative Commons Attribution-NonCommercial License](#), which permits use, distribution and reproduction in any medium, provided the original work is properly cited and is not used for commercial purposes.

Wintertime Supraglacial Lake Drainage Cascade Triggers Large-Scale Ice Flow Response in Greenland

Nathan Maier^{1,2} , Jonas Kvist Andersen³, Jérémie Mouginit^{1,4} , Florent Gimbert¹, and Olivier Gagliardini¹

¹Université Grenoble Alpes, CNRS, IGE, Grenoble, France, ²Now at Los Alamos National Laboratory, Los Alamos, NM, USA, ³DTU Space, Technical University of Denmark, Lyngby, Denmark, ⁴Department of Earth System Science, University of California-Irvine, Irvine, CA, USA

Abstract Surface melt forces summertime ice-flow accelerations on glaciers and ice sheets. Here, we show that large meltwater-forced accelerations also occur during wintertime in Greenland. We document supraglacial lakes (SGLs) draining in cascades at unusually high elevation, causing an expansive flow acceleration over a ~5,200 km² region during winter. The three-component interferometric surface velocity field and decomposition modeling reveal the underlying flood propagation with unprecedented detail as it traveled over 160 km from the drainage site to the margin, providing novel constraints on subglacial water pathways, drainage morphology, and links with basal sliding. The triggering SGLs continuously grew over 40 years and suddenly released decades of stored meltwater, demonstrating surface melting can impact dynamics well beyond melt production. We show these events are likely common and thus their cumulative impact on dynamics should be further evaluated.

Plain Language Summary Understanding factors that influence flow speeds on ice sheets are linked to our ability to predict changes in sea level and prepare coastal communities for the future. On the Greenland Ice Sheet, ice flow-speed changes have long been linked to surface melting in summer. Meltwater can make it to the bed of the ice sheet via surface cracks causing changes in ice motion. Here, we show that melt that is produced during summer, but stored within lakes on the ice surface, can drain to the bed and cause large flow accelerations during winter. This demonstrates the influence of meltwater on flow speeds needs to be considered beyond when it is produced.

1. Introduction

The annual velocity cycle along the margins of Greenland is closely linked to meltwater availability (Andrews et al., 2018; Bartholomew et al., 2010; Hoffman et al., 2011; Sole et al., 2013; Van de Wal et al., 2015). In early summer, the ice sheet accelerates as surface meltwater is delivered to the bed and is routed through an inefficient subglacial drainage system favoring high basal water pressures (Andrews et al., 2018; Bartholomew et al., 2010; Hoffman et al., 2011). In late summer, drainage efficiency gains cause water pressures to decrease, decelerating the ice sheet back to or below the previous winter values (Andrews et al., 2018; Bartholomew et al., 2010; Hoffman et al., 2011; Sole et al., 2013; Van de Wal et al., 2015). In the absence of surface melt during the winter period, flow speed typically follows a monotonic increase (Harper et al., 2021; Van de Wal et al., 2015), which is attributed to decreasing ice-bed coupling from in situ production of basal melt (Harper et al., 2021). This cycle is the basis of current understanding of hydrology-dynamic coupling and how increased melting will influence flow speeds and mass loss in the future (Davison et al., 2019).

Large transient changes in surface velocities are not typically expected during winter due to the absence of surface melt. Yet, perennial water storage of the previous summer's meltwater can occur within supraglacial lakes (SGLs) that remain partially unfrozen through winter (Benedek & Willis, 2021; Koenig et al., 2015; Lampkin et al., 2020; Law et al., 2020; Schröder et al., 2020). Recent work indicates isolated SGLs can drain during winter (Benedek & Willis, 2021; Schröder et al., 2020), but current evidence does not suggest a significant impact on flow speeds (Benedek & Willis, 2021). This contrasts with observations made during summer, where SGL drainages, and particularly drainage clusters, can drive multi-day accelerations across large areas due to the friction reduction as the rapid influx of water to the bed drains downgradient (Andrews et al., 2018; Christoffersen et al., 2018; Hoffman et al., 2018; Mejía et al., 2021).

Writing – review & editing: Florent
Gimbert, Olivier Gagliardini

Here, we document a cascading SGL drainage that generates an expansive flow acceleration wave during winter in western Greenland (Figure 1). We decompose the motion into its horizontal and vertical components and perform surface deformation modeling to determine likely flow pathways and drainage characteristics as the flood wave propagates to the margin. Finally, we document the historical SGL growth that enabled the incipient drainages, hypothesize triggering mechanisms, and put the dynamic impact in the context of long-term change.

2. Methods

2.1. DInSAR Velocities

We use Sentinel-1 image pairs with a 6-day temporal baseline from three tracks (T90, T25, and T127) to generate line-of-sight (LoS) velocity maps before, during, and after the lake drainages following the approaches outlined in Andersen et al. (2020) and Kusk et al. (2021). Velocities were derived using differential SAR Interferometry (DInSAR), which exploits the difference in phase signal between subsequent acquisitions. Although DInSAR only retrieves a single component of the velocity vector and is limited to regions in which interferometric coherence is retained, the measurement accuracy and spatial resolution is significantly higher (~ 0.5 m/yr vs. tens of m/yr difference in accuracy, order of magnitude higher spatial resolution) than that obtained with tracking-based measurements (Andersen et al., 2020).

2.2. Identifying Winter SGL Drainages

We manually identified 15 winter SGL drainages during March of 2018 using all Sentinel-2 (ESA) and Landsat 8 (USGS) optical imagery acquired for the region between 15th February and 29th April 2018. The frozen lake surfaces are near roughness-free, making them readily identifiable from surrounding regions (Figure S1 in Supporting Information S1). SGL drainages are identified via the abrupt change from smooth surfaces to collapse basins or rough lakebeds from scene to scene. We interpret the former to result from the loss of mechanical support provided by the underlying water, indicating drainage or partial drainage of the lake below the ice lid via hydrofracture. Similar surface features and interpretation were used to confirm winter drainage detection using other methods (Benedek & Willis, 2021; Schröder et al., 2020).

2.3. Decomposing Vertical and Horizontal Motion

We exploit the fact that DInSAR measurements are sensitive to both horizontal and vertical motion to decompose the velocity into vertical and horizontal components for select time periods during the drainage cascade. Estimating the three-dimensional velocity vector requires three spatiotemporally overlapping tracks with different viewing geometries. The satellite coverage does not allow this, and we instead use data from one ascending and one descending Sentinel-1 track (T90 and T25) to estimate two components of the velocity: horizontal speed in the flow direction, u_{FD} , and vertical speed, u_v . We use the PROMICE average velocity map (2016–2019; Solgaard et al., 2021) to constrain the flow direction and assume it remains constant during the event. The measured LoS motion from each track can then be decomposed using a system of equations:

$$u_{LoS,asc} = \cos \alpha_{asc} \cos \theta_{asc} u_{FD} + \sin \theta_{asc} u_v \quad (1a)$$

$$u_{LoS,dsc} = \cos \alpha_{dsc} \cos \theta_{dsc} u_{FD} + \sin \theta_{dsc} u_v \quad (1b)$$

where $\alpha = \beta - \phi$ is the angle between the horizontal flow angle, β , and the ground-projected radar LoS (described by the angle ϕ), and is the elevation angle between the LoS and its ground projection. We use Equations 1a–1b to solve for the two unknowns, u_{FD} and u_v . The temporal overlap between the chosen tracks is 4.5 days, meaning that some uncertainty is added by the fact that the two measurement periods do not perfectly overlap. Given the relatively slow velocity of the propagating wave (< 0.1 m/s), we expect the displacement to be similar between image scenes. We test this assumption and our inference of uplift by decomposing a synthetic wave model constrained by the observations (Section 2.4).

To reduce the noise from spatially correlated errors specific to each track, we estimate the change in, rather than absolute velocities resulting from the drainage event. Hence, Equations 1a–1b become:

$$du_{LoS,asc} = \cos \alpha_{asc} \cos \theta_{asc} du_{FD} + \sin \theta_{asc} du_v \quad (2a)$$

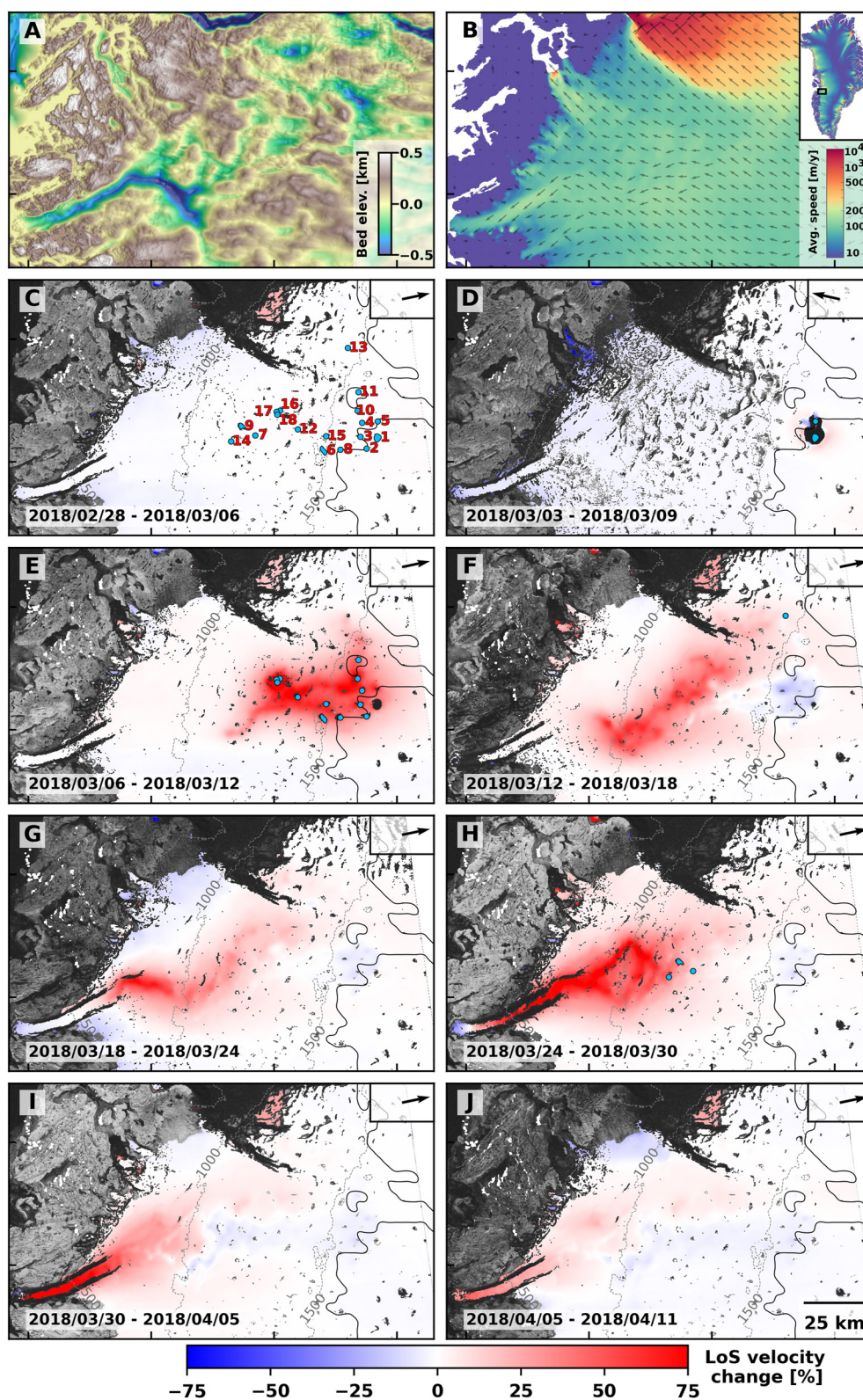


Figure 1.

$$du_{\text{LoS,dsc}} = \cos \alpha_{\text{dsc}} \cos \theta_{\text{dsc}} du_{\text{FD}} + \sin \theta_{\text{dsc}} du_v \quad (2b)$$

where du_{LoS} is the difference between the measured LoS velocity field and a reference field (taken as a DInSAR LoS measurement from the same track prior to the SGL drainages).

2.4. Synthetic Wave Model

To evaluate how the assumptions made to decompose the LoS velocities may bias the retrieved horizontal and vertical velocity fields, we decompose a synthetic coupled horizontal and vertical displacement wave using the same procedure as described in Section 2.3 for the observed data. We model a coupled horizontal and vertical flowline velocity wave, which mimics a horizontal flow increase driven by bed separation, as Gaussian kernels propagating across a 160 km flowline using a kernel width (σ) and wave speed constrained by our data. We then calculate the accumulated horizontal displacement and change in uplift that would occur between the two 6-day windows that overlap by 4.5 days to match the interval between the T90 and T25 orbital tracks. Finally, we decompose the signal using the mean orbital parameters from the T90 and T25 tracks and compare the results to the decomposed fields to constrain the conditions required to reproduce the major features of the data.

3. Results and Discussion

3.1. Wintertime SGL Drainage Cascade

On approximately 9th March 2018, two SGLs (1 and 2) drained in a land-terminating sector just south of Jakobshavn Isbræ 142 km inland from the westernmost ice margin and at high elevations ($\sim 1,600$ m; Figure 1 and Figure S1 in Supporting Information S1). This altitude corresponds to the multi-year snowline (Vandecrux et al., 2019), which approximates the transition between the accumulation and ablation zones. Before the event, no observable acceleration is detected. These incipient drainages trigger an acceleration in the direct vicinity of the draining lakes marking the initiation of a marginally propagating velocity wave.

Between 9th and 12th March, eight additional SGLs (3–12) drained ~ 40 km downstream and ~ 20 km north of the original drainage cluster (Figure 1e and Figure S1 in Supporting Information S1). During this period, LoS velocities increase up to 160% of pre-drainage values. The wave exhibits a complex structure and bifurcates into two main paths. The wave heading west propagates toward Nordenskiöld Glacier, a relatively slow-moving outlet glacier (~ 200 m/yr). This western path shows multiple branches emanating from the northern and southern part of the original drainage cluster that coalesce downglacier later on. The wave heading north propagates toward Jakobshavn Isbræ, the fastest marine-terminating outlet glacier in Greenland (> 10 km/yr), along a single branch (Figure 1). The velocity branches always closely follow the troughs in the bed topography.

As the event continues, the westward wavefront continues to move downglacier and again shows a complex multi-branched structure following bed depressions (Figure 1f). The northernmost wavefront is no longer clearly visible, extending beyond the useable DInSAR observations. The westward branches eventually coalesce ~ 80 km downglacier from the original drainage site. LoS velocities within the main wave remain 160% of their background value. Between 18th and 24th March, the westward wavefront enters the main Nordenskiöld trough, and velocities increase to $\sim 250\%$ above background (Figure 1g). Between 24th and 30th March, three more SGLs (13–15) are observed to drain about 60 km upglacier of the wavefront (Figure 1h). This drainage causes an additional acceleration following an angular bed trough to the north which rejoins the main wave path before entering the Nordenskiöld bed trough. The wavefront reaches the terminus of Nordenskiöld between 30th March and 4th April, ~ 25 days after its initiation. This timing coincides with the proglacial release of water from Nordenskiöld proglacial delta observed in optical imagery (Figure S2 in Supporting Information S1).

Figure 1. Winter drainage cascade and dynamic response—panels (a and b) show bed elevation (Morlighem, 2018; Morlighem et al., 2017) and 1995–2016 average velocity (Mouginot et al., 2019). Remaining panels show the change in line-of-sight (LoS) velocity (relative to a pre-event acquisition) from Sentinel-1 interferometric (DInSAR) measurements (Section 2.1) overlaid on corresponding coherence images. Panel (c) shows the location of all lakes inferred to have completely or partially drained (blue polygons, or dots for lakes smaller than 4 km^2) along with the velocity anomaly field pre-drainage. The following panels show the sequence of lake drainages and the propagation of the resulting velocity wave. Lakes appear when they are inferred to drain, coincident with the period of the velocity acquisition. Velocity changes are measured from Sentinel-1 tracks 90 (panels (c and e–j)) and 127 (panel (d)). The black arrow indicates ground-projected LoS, dashed lines indicate surface elevation contours (I. Howat & Ohio State University, 2017; I. Howat, Ohio State University, & Byrd Polar Research Center, 2017; I. M. Howat et al., 2014), and the solid line indicates the time-averaged snowline (Vandecrux et al., 2019).

3.2. Drainage Characteristics Revealed by Decomposition of the Velocity Field

Using the approach outlined in Section 2.3, we invert for horizontal motion (relative to pre-drainage velocities) and the vertical displacement and find they exhibit strikingly distinct patterns (Figure 2 and Figure S3 in Supporting Information S1). The horizontal velocity field is smooth and spatially extends over 10–50 km in flow-perpendicular width, while the uplift is concentrated in a bead and thread structure with a characteristic width of <10 km, where high uplift patches (~0.25 m) are linked together through thinner uplift connectors of lower amplitude.

Synthetic modeling validates the decomposition assumptions and the interpretation that the decomposed fields mainly represent horizontal and vertical motion (Figure 2; Section 2.4). We find the best fit to the decomposed data is a horizontal (amplitude = 60 m/yr) and vertical uplift/bed separation wave (amplitude = 0.25 m) propagating at 0.08 m/s, all values within the constraints of the data. This fit indicates the horizontal velocity wave is wider ($\sigma = 15$ km) and precedes the uplift wave ($\sigma = 10$ km) by 15 km. These parameters capture the phase relationship between the peaks as well as the pre- and post-wave dips in vertical displacement observed in the decomposed fields. The phase difference between the decomposed and synthetic waves, as well as the pre-wave dip in vertical displacement indicates the fields are somewhat distorted compared to the original values due to the mismatch in temporal overlap. However, we still find we can clearly distinguish horizontal motion and vertical displacement, allowing us to infer vertical and horizontal fields from the decomposed data shown in Figure 2a.

Following the results of the modeling, we interpret the uplift and subsidence, which produces the complex structure in Figure 1, as changes in bed separation that identify likely flow pathways (Figure 2 and Figure S4 in Supporting Information S1) as the ~0.18 km³ of meltwater (Supporting Information) injected into the ice-bed interface drains toward the margin. This is supported by the following evidence: (a) neither vertical motion resulting from vertical strain or bed tangential motion are likely to produce such a pattern (Figure S5 in Supporting Information S1); (b) the uplifted branches correspond to hydropotential lows within the bed troughs, which is the expected pathway of subglacially draining water (Figure 1a and Figure S6 in Supporting Information S1); (c) regions of highest uplift correspond to depressions in the hydropotential (subglacial sinks; Figure S7 in Supporting Information S1). The bead and thread uplift structure suggests a fill and spill drainage style similar to the drainage of subglacial lakes (Dow et al., 2016; Livingstone et al., 2016), with water captured by each sink along the flow path released when the pressure reaches the hydropotential lip of each depression. Drainage through these regions requires overpressure, which can physically cause bed separation either due to the detachment of the ice base via floatation or cavity formation via ice creep and enhanced sliding (Andrews et al., 2018; Bartholomew et al., 2008; Bartholomew et al., 2010; Cowton et al., 2016; Gagliardini et al., 2007; Helanow et al., 2021; Hoffman et al., 2011), and is thus consistent with the beads of high uplift (Figure 2 and Figure S7 in Supporting Information S1). We note since SGLs, hydropotential depressions and subglacial lakes are often collocated (Fan et al., 2022), the drainage, as well as the uplift and subsidence, could also be partly modulated by subglacial lakes.

The comparatively smooth and expansive extent of the horizontal field indicates much of the horizontal acceleration is not directly related to bed separation. We posit that the changes in bed friction are linked to bed separation as conceptualized by Gagliardini et al. (2007), Gilbert et al. (2022), Gimbert et al. (2021), Schoof (2005), and Tsai et al. (2022) and more expansive changes in dynamics occur through stress transmission within the ice—a behavior inferred previously from scarce in situ measurement and modeling (Andrews et al., 2014; Derkacheva et al., 2021; Hoffman et al., 2016; Maier et al., 2021; Ryser et al., 2014) but never documented observationally. Alternatively changes in bed friction could be generated via water pressure increases emanating beyond the uplifted region. We suggest this scenario is less likely given subglacial observations show pressure communication typically occurs only across short distances (Andrews et al., 2014; Rada & Schoof, 2018).

We estimate the speed of the velocity wave that propagates along the main Nordenskiöld drainage pathway (Figure S4 in Supporting Information S1) to be between 0.03 and 0.17 m s⁻¹ (Figure 3, Supporting Information). This velocity is consistent with repeat dye tracer experiments in Greenland which show seasonally evolving drainage velocities which increase ~0.1 to ~1 m/s as the melt season progresses (Chandler et al., 2013). This increase was inferred to reflect the transition from inefficient to efficient drainage pathways. Our event-averaged drainage velocity of ~0.1 m/s and 1–10 km scale of the uplifted regions would imply drainage mainly through inefficient and distributed drainage pathways rather than through channelized or turbulent sheet components where drainage speeds are expected to be >1 m/s (Chandler et al., 2013; Tsai & Rice, 2010). Even so, given

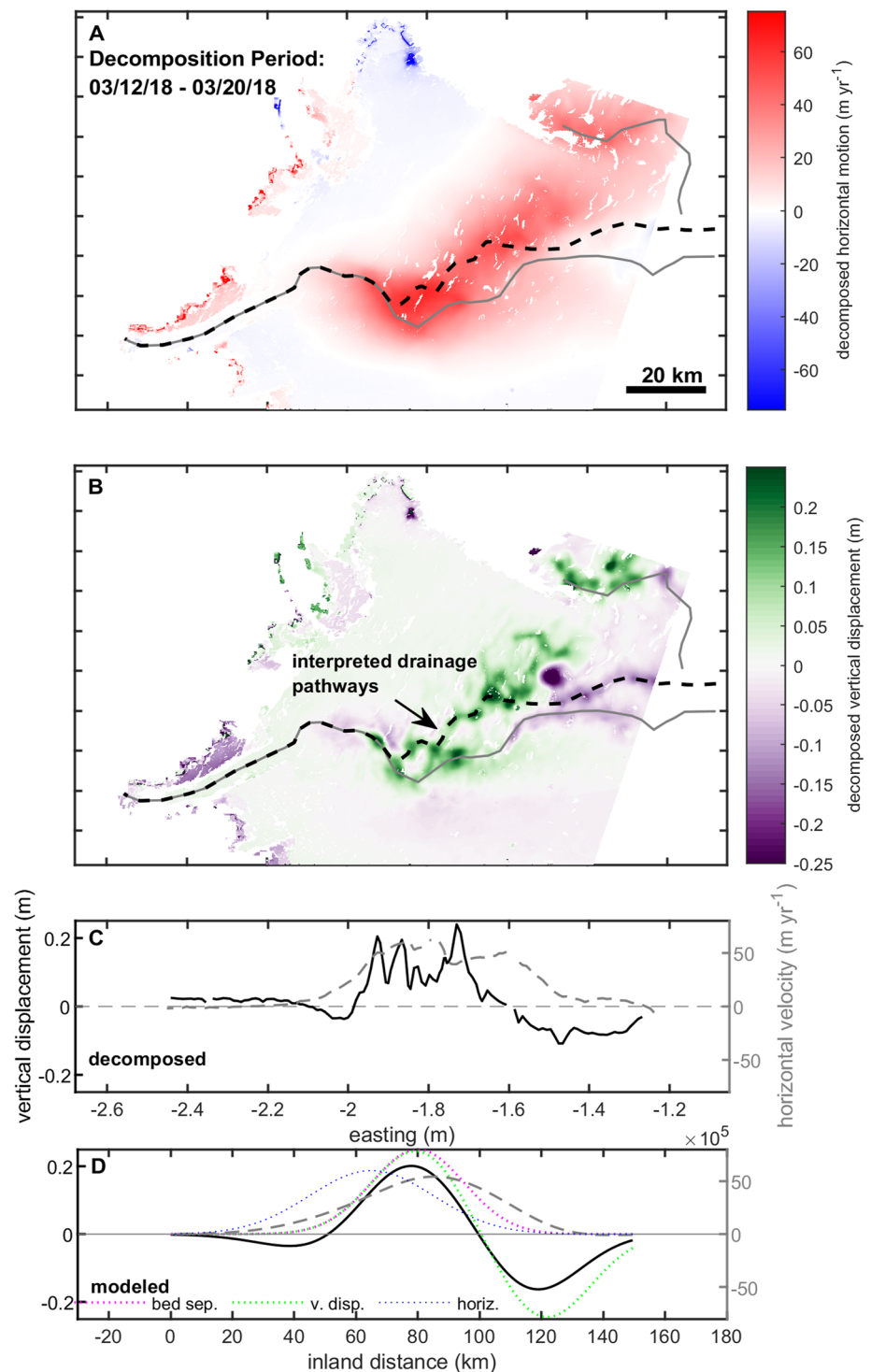


Figure 2. Decomposed motion—snapshot of decomposed horizontal motion (relative to pre-drainage velocities) (a) and vertical surface displacement (b) during drainage event. The three interpreted flow pathways are shown with solid gray and black dashed lines. (c) Decomposed horizontal (gray dashed) and vertical (solid black) motion along the center flowline (dashed black line in panel (c)). (d) Decomposition (horizontal motion - gray dashed, vertical displacement/change in uplift over 6-day window - solid black) of synthetic velocity wave (dotted blue) and uplift wave (dotted pink, vertical displacement - dotted green) with characteristics constrained by the data (Sections 2.3–2.4).

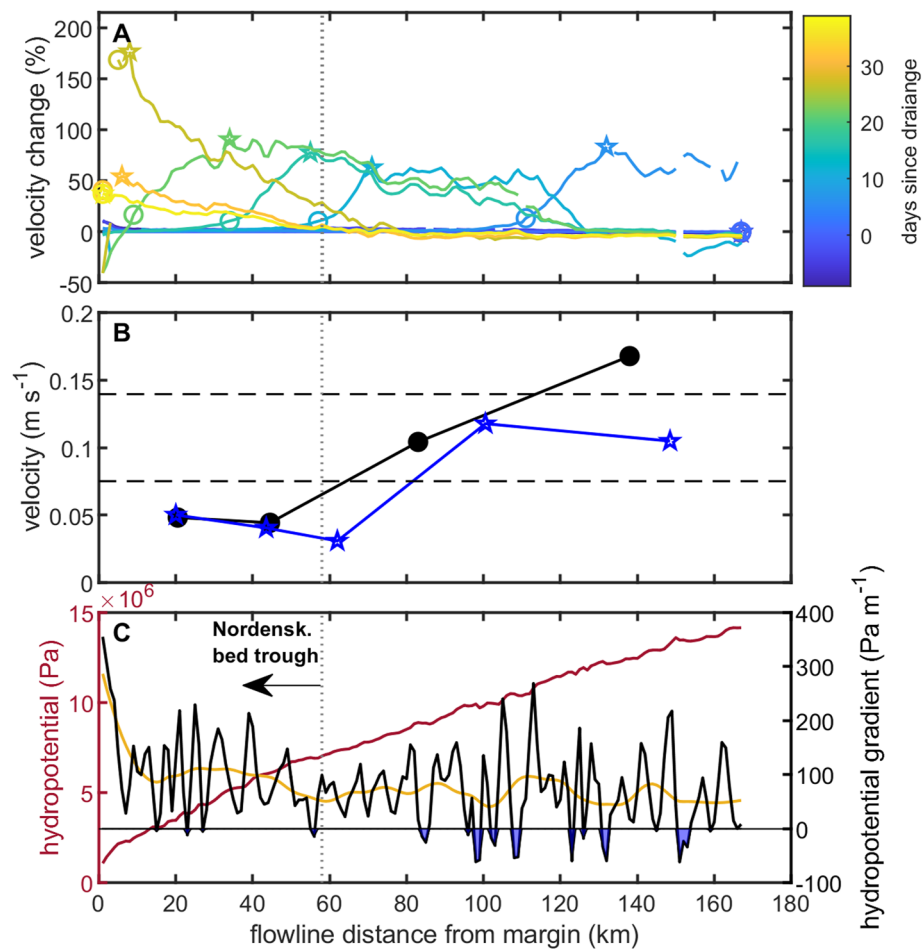


Figure 3. Subglacial drainage characteristics—(a) percent velocity changes along one of the inferred Nordenskiöld drainage pathways (black dashed line Figure 2) as the velocity wave propagates to the margin (right to left). Stars show tracked wave peaks and circles show tracked wavefronts (Supporting Information). (b) Estimated wave velocity using the tracked peaks (stars) and fronts (circles). Velocity marker is shown at the mid-point between the two tracked peaks or fronts used to estimate the speed. Dashed bounds show event-integrated drainage velocity inferred from optical imagery (Figure S2 in Supporting Information S1). (c) Left axis shows hydropotential (maroon line) assuming ice-overburden pressure, right-axis shows hydropotential gradients (black line), and smoothed hydropotential gradients (orange line) along flowline. Blue shading shows the location of hydropotential depressions.

the spatiotemporal averaged nature of the velocities and varying hydropotential gradient, it is plausible many drainage styles could have manifested at some point along the drainage path. The drainage speed slows to about 0.05 m/s as the water enters the Nordenskiöld trough while horizontal velocities increase by 250% even though modeled hydropotential gradients are high and no modeled subglacial sinks are present (Figure 3). This implies the drainage system conductivity is lower within the trough possibly due to the accumulation of sediments, where water drains mainly via Darcian flow, or to differences in the pre-existing drainage system geometry.

3.3. Hypothesized Trigger Mechanisms

In the absence of surface melting which can cause SGL overflow, the drainages likely occur due to hydrofracture to the ice base (Chudley et al., 2019; Das et al., 2008; Stevens et al., 2015). The initial formation of crevasses necessary for hydrofracture requires precursor events that generate tensile stress transients (Christoffersen et al., 2018; Stevens et al., 2015). Here, no precursor is directly observed (Figure 1), however it is possible that a short duration event would not be detected in our 6-day velocity maps. Yet, the initially draining lakes are located near the snowline (Figure 1) and are far inland from the terminus of any outlet glacier, which would be the most likely place for large transients to originate during winter. Given this, we suggest several other plausible ways the

incipient drainage could occur: (a) a stress transient and surface fracture could have occurred due to a local stick-slip event, subglacially draining lake, or transient drainage connection; (b) an upgradient crevasse could migrate into the SGL, negating the need for concurrent crevasse formation; (c) rapid cooling could thermally fracture the ice surface adjacent to the incipient SGL (Podolskiy et al., 2019). Evaluating these hypotheses will ultimately require more detailed data than is presented here, however we note that no visible crevasses were found near the incipient lake drainages.

Once the initial lake drainage has started, the resulting ice displacements can generate stress transients that can trigger hydrofracture within nearby lakes (Christoffersen et al., 2018; Doyle et al., 2013; Tedesco et al., 2013), thus initiating a cascade of SGL drainages near the original drainage location. Interestingly, many drainages occur more than 40 km away from and up to 14 days after the original drainage. This would indicate that their drainage is unrelated to stress transients caused by ice-tectonic deformations around the incipient drainages and are tapped after the velocity wave passes and tensile stress conditions are favorable for hydrofracture.

3.4. Decadal Scale-Storage and Release of Meltwater

Tracking the evolution of the SGLs since 1972 to estimate the changes in their area through time (Figure 4 and Figure S10 in Supporting Information S1) reveals many of these lakes formed and grew for years to decades before initially draining, and for the two of the highest elevation lakes (Lakes 1 and 3), this was the first observed instance of drainage after a half-century of growth (Figure 4). This suggests that events like these, where high-elevation SGLs drain and trigger an expansive downgradient acceleration, are linked to increases in melt production which promote the formation and growth of high-elevation lakes (Leeson et al., 2015). The historical lake evolution records (Figure 4 and Figure S8 in Supporting Information S1) also show that once drained, lakes appear to drain more frequently thereafter; indicating initial SGL drainage might play a role in establishing persistent surface-to-bed connections where there were none prior.

3.5. Implications for Long-Term Ice Flow

Recent work suggests persistent basal water storage has a prominent role in the centennial-scale evolution of the Greenland Ice Sheet (Maier et al., 2022). Although well-studied (Davison et al., 2019), the specifics of how and when water is stored at the base remains elusive. Here, we show melt-forced coupling changes can occur during winter, which for this event increases annual ice discharge by 1%–4% (Figure S9 in Supporting Information S1) compared to if the event did not occur. Further, flow velocities before and after the flood wave passes shows regions around the drainage pathway have slowed upstream of the Nordenskiöld by 5%–10% while within the Nordenskiöld they have increased by 10%–20% (Figure 1j), implying commensurate changes in subglacial water storage due to the passing of the subglacial flood. These factors suggest events like these have the potential to impact multi-annual velocity variability and could potentially precondition the drainage system for the following summer and have a broader impact on dynamics in a way not resolved in this analysis. Yet, given the spatio-temporally isolated nature of the event and modest impact on ice flow, events like these would have to occur frequently to have a substantial impact on marginal dynamics. Undertaking a precursory search in the vicinity of Nordenskiöld glacier during the following years (2019–2021), we identified four additional winter drainage events with associated dynamic changes (Figures S10 and S11 in Supporting Information S1), suggesting winter-time transients are common within this region and necessitate further study to assess their cumulative ice-sheet-wide impact.

4. Conclusion

Our finding links expansive flow changes during winter to summer meltwater production, demonstrating surface melt can have a prolonged influence on dynamics that persists beyond when it is generated. Moreover, we demonstrate this lag can be up to decades, meaning the hydrology-dynamic cycle, which is usually considered on an annual and seasonal basis, can operate on fundamentally different timescales. The unique winter timing and high-resolution nature of the data revealed drainage structure and the link between uplift and sliding across scales not achievable via in-situ studies. Thus, in addition to establishing the impact of winter SGL drainages and triggering mechanisms, future work should seek to leverage events like these to provide key constraints on hydrologically driven transient-friction changes.

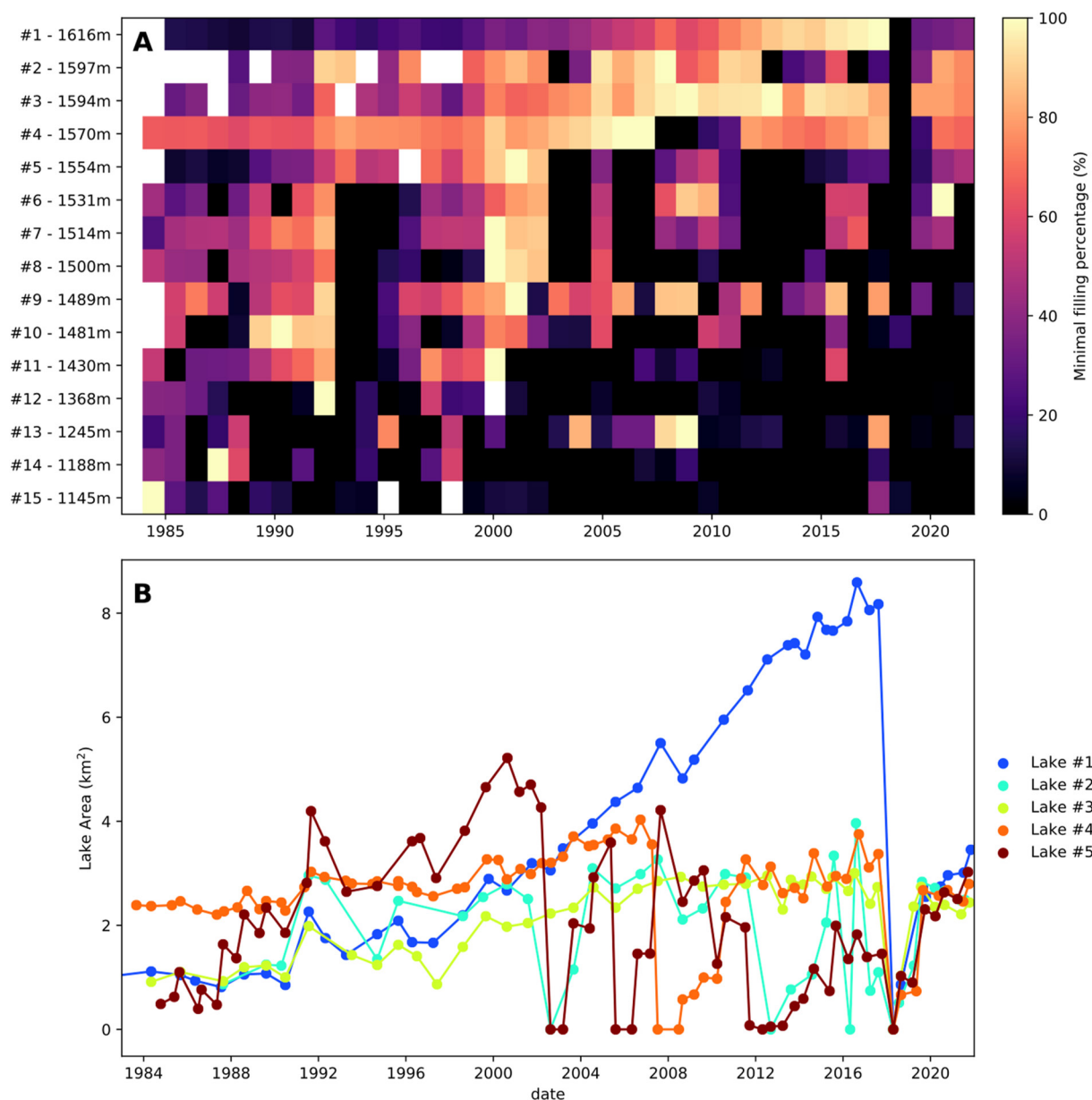


Figure 4. Multi-decadal SGL evolution—(a) the percent fill of the supraglacial lakes (SGLs) since 1983 relative to the largest area observed over the 1983–2022 period is shown. Where multiple areas are estimated for a year, the minimum value is shown, which generally indicates that the lake emptied in that year. The lake contours used to calculate the area are digitized from the Landsat archive (Supporting Information). The altitude of each SGL is indicated next to the lake number. (b) The area of the five highest SGLs in elevation as a function of time is plotted (all SGL shown in Figure S8 in Supporting Information S1). We note Lake 1 could be identified all the way back to 1972.

Conflict of Interest

The authors declare no conflicts of interest relevant to this study.

Data Availability Statement

All data used to generate this manuscript is publicly available for download. Ice surface elevation: <https://doi.org/10.5067/H0KUYVF53Q8M>, Land/Ice classification: <https://doi.org/10.5067/B8X58MQBFUPA>, Bed topography: <https://doi.org/10.5067/2CIX82HUV88Y>, Snowline elevation: <https://doi.org/10.18739/A2V40JZ6C>, Sentinel-1 and Sentinel-2: <https://scihub.copernicus.eu/>, Landsat: <https://earthexplorer.usgs.gov/>, ArcticDEM:

doi.org/10.7910/DVN/OHHUKH. Figures 2–4 were produced with MATLAB vR2019B. Figure 1 was produced with Matplotlib v3.5.0.

Acknowledgments

The authors dedicate this work to our dear friend and colleague Jérémie Mouginot who recently passed away. He will always be remembered for his kindness and enthusiasm he brought to his science and those around him. This work was funded by the French National Research Agency Grants ANR-19-CE01-0011-01 and ANR-17-CE01-0008 and the French space agency (CNES). J.K.A. acknowledges support from DTU Space.

References

- Andersen, J. K., Kusk, A., Boncori, J. P. M., Hvidberg, C. S., & Grinsted, A. (2020). Improved ice velocity measurements with Sentinel-1 TOPS interferometry. *Remote Sensing*, 12(12), 2014. <https://doi.org/10.3390/rs12122014>
- Andrews, L. C., Catania, G. A., Hoffman, M. J., Gulley, J. D., Lüthi, M. P., Ryser, C., et al. (2014). Direct observations of evolving subglacial drainage beneath the Greenland Ice Sheet. *Nature*, 514(7520), 80–83. <https://doi.org/10.1038/nature13796>
- Andrews, L. C., Hoffman, M. J., Neumann, T. A., Catania, G. A., Lüthi, M. P., Hawley, R. L., et al. (2018). Seasonal evolution of the subglacial hydrologic system modified by supraglacial lake drainage in western Greenland. *Journal of Geophysical Research: Earth Surface*, 123(6), 1479–1496. <https://doi.org/10.1029/2017j004585>
- Bartholomew, T. C., Anderson, R. S., & Anderson, S. P. (2008). Response of glacier basal motion to transient water storage. *Nature Geoscience*, 1(1), 33–37. <https://doi.org/10.1038/ngeo.2007.52>
- Bartholomew, I., Nienow, P., Mair, D., Hubbard, A., King, M. A., & Sole, A. (2010). Seasonal evolution of subglacial drainage and acceleration in a Greenland outlet glacier. *Nature Geoscience*, 3(6), 408–411. <https://doi.org/10.1038/ngeo863>
- Benedek, C. L., & Willis, I. C. (2021). Winter drainage of surface lakes on the Greenland Ice Sheet from Sentinel-1 SAR imagery. *The Cryosphere*, 15(3), 1587–1606. <https://doi.org/10.5194/tc-15-1587-2021>
- Chandler, D., Wadhwa, J., Lis, G., Cowton, T., Sole, A., Bartholomew, I., et al. (2013). Evolution of the subglacial drainage system beneath the Greenland Ice Sheet revealed by tracers. *Nature Geoscience*, 6(3), 195–198. <https://doi.org/10.1038/ngeo1737>
- Christoffersen, P., Bougamont, M., Hubbard, A., Doyle, S. H., Grigsby, S., & Pettersson, R. (2018). Cascading lake drainage on the Greenland Ice Sheet triggered by tensile shock and fracture. *Nature Communications*, 9(1), 1–12. <https://doi.org/10.1038/s41467-018-03420-8>
- Chudley, T. R., Christoffersen, P., Doyle, S. H., Bougamont, M., Schoonman, C. M., Hubbard, B., & James, M. R. (2019). Supraglacial lake drainage at a fast-flowing Greenlandic outlet glacier. *Proceedings of the National Academy of Sciences*, 116(51), 25468–25477. <https://doi.org/10.1073/pnas.1913685116>
- Cowton, T., Nienow, P., Sole, A., Bartholomew, I., & Mair, D. (2016). Variability in ice motion at a land-terminating Greenlandic outlet glacier: The role of channelized and distributed drainage systems. *Journal of Glaciology*, 62(233), 451–466. <https://doi.org/10.1017/jog.2016.36>
- Das, S. B., Joughin, I., Behn, M. D., Howat, I. M., King, M. A., Lizarralde, D., & Bhatia, M. P. (2008). Fracture propagation to the base of the Greenland Ice Sheet during supraglacial lake drainage. *Science*, 320(5877), 778–781. <https://doi.org/10.1126/science.1153360>
- Davison, B. J., Sole, A. J., Livingstone, S. J., Cowton, T. R., & Nienow, P. W. (2019). The influence of hydrology on the dynamics of land-terminating sectors of the Greenland Ice Sheet. *Frontiers of Earth Science*, 7, 10. <https://doi.org/10.3389/feart.2019.00010>
- Derkacheva, A., Gillet-Chaulet, F., Mouginot, J., Jager, E., Maier, N., & Cook, S. (2021). Seasonal evolution of basal environment conditions of Russell sector, west Greenland, inverted from satellite observation of surface flow. *The Cryosphere*, 15(12), 5675–5704. <https://doi.org/10.5194/tc-15-5675-2021>
- Dow, C. F., Werder, M. A., Nowicki, S., & Walker, R. T. (2016). Modeling Antarctic subglacial lake filling and drainage cycles. *The Cryosphere*, 10(4), 1381–1393. <https://doi.org/10.5194/tc-10-1381-2016>
- Doyle, S. H., Hubbard, A. L., Dow, C. F., Jones, G. A., Fitzpatrick, A. A. W., Gusmeroli, A., et al. (2013). Ice tectonic deformation during the rapid in situ drainage of a supraglacial lake on the Greenland Ice Sheet. *The Cryosphere*, 7(1), 129–140. <https://doi.org/10.5194/tc-7-129-2013>
- Fan, Y., Ke, C.-Q., Shen, X., Xiao, Y., Livingstone, S. J., & Sole, A. J. (2022). Subglacial lake activity beneath the ablation zone of the Greenland Ice Sheet. *The Cryosphere Discussions*, 1–16.
- Gagliardini, O., Cohen, D., Råback, P., & Zwinger, T. (2007). Finite-element modeling of subglacial cavities and related friction law. *Journal of Geophysical Research: Earth Surface*, 112(F2), F02027. <https://doi.org/10.1029/2006JF000576>
- Gilbert, A., Gimbert, F., Thøgersen, K., Schuler, T. V., & Käbb, A. (2022). A consistent framework for coupling basal friction with subglacial hydrology on hard-bedded glaciers. *Geophysical Research Letters*, 49(13), e2021GL097507. <https://doi.org/10.1029/2021gl097507>
- Gimbert, F., Gilbert, A., Gagliardini, O., Vincent, C., & Moreau, L. (2021). Do existing theories explain seasonal to multi-decadal changes in glacier basal sliding speed? *Geophysical Research Letters*, 48(15), e2021GL092858. <https://doi.org/10.1029/2021gl092858>
- Harper, J., Meierbachtol, T., Humphrey, N., Saito, J., & Stansberry, A. (2021). Generation and fate of basal meltwater during winter, western Greenland Ice Sheet. *The Cryosphere*, 15(12), 5409–5421. <https://doi.org/10.5194/tc-15-5409-2021>
- Helanow, C., Iverson, N. R., Woodard, J. B., & Zoet, L. K. (2021). A slip law for hard-bedded glaciers derived from observed bed topography. *Science Advances*, 7(20), eabe7798. <https://doi.org/10.1126/sciadv.abe7798>
- Hoffman, M. J., Andrews, L. C., Price, S. F., Catania, G. A., Neumann, T. A., Lüthi, M. P., et al. (2016). Greenland subglacial drainage evolution regulated by weakly connected regions of the bed. *Nature Communications*, 7(1), 13903. <https://doi.org/10.1038/ncomms13903>
- Hoffman, M. J., Catania, G. A., Neumann, T., Andrews, L., & Rumrill, J. (2011). Links between acceleration, melting, and supraglacial lake drainage of the western Greenland Ice Sheet. *Journal of Geophysical Research: Earth Surface*, 116(F4), F04035. <https://doi.org/10.1029/2010j001934>
- Hoffman, M. J., Perego, M., Andrews, L. C., Price, S. F., Neumann, T. A., Johnson, J. V., et al. (2018). Widespread moulin formation during supraglacial lake drainages in Greenland. *Geophysical Research Letters*, 45(2), 778–788. <https://doi.org/10.1002/2017gl075659>
- Howat, I., & Ohio State University. (2017). MEaSUREs Greenland Ice Mapping Project (GIMP) digital elevation model from GeoEye and WorldView imagery, version 1 [Dataset]. NASA National Snow and Ice Data Center DAAC. <https://doi.org/10.5067/H0KUYVF53Q8M>
- Howat, I., Ohio State University, & Byrd Polar Research Center. (2017). MEaSUREs Greenland Ice Mapping Project (GIMP) land ice and ocean classification mask, version 1 [Dataset]. NASA National Snow and Ice Data Center DAAC. <https://doi.org/10.5067/B8X58MQBFUPA>
- Howat, I. M., Negrete, A., & Smith, B. E. (2014). The Greenland Ice Mapping Project (GIMP) land classification and surface elevation data sets. *The Cryosphere*, 8(4), 1509–1518. <https://doi.org/10.5194/tc-8-1509-2014>
- Koenig, L. S., Lampkin, D., Montgomery, L., Hamilton, S., Turrin, J., Joseph, C., et al. (2015). Wintertime storage of water in buried supraglacial lakes across the Greenland Ice Sheet. *The Cryosphere*, 9(4), 1333–1342. <https://doi.org/10.5194/tc-9-1333-2015>
- Kusk, A., Andersen, J. K., & Boncori, J. M. (2021). Sentinel-1 TOPS interferometry for ice flow mapping. In *Presented at the EUSAR 2021; 13th European Conference on Synthetic Aperture Radar* (pp. 1–5). VDE.
- Lampkin, D. J., Koenig, L., Joseph, C., & Box, J. E. (2020). Investigating controls on the formation and distribution of wintertime storage of water in supraglacial lakes. *Frontiers of Earth Science*, 370. <https://doi.org/10.3389/feart.2020.00370>
- Law, R., Arnold, N., Benedek, C., Tedesco, M., Banwell, A., & Willis, I. (2020). Over-winter persistence of supraglacial lakes on the Greenland Ice Sheet: Results and insights from a new model. *Journal of Glaciology*, 66(257), 362–372. <https://doi.org/10.1017/jog.2020.7>

- Leeson, A., Shepherd, A., Briggs, K., Howat, I., Fettweis, X., Morlighem, M., & Rignot, E. (2015). Supraglacial lakes on the Greenland ice sheet advance inland under warming climate. *Nature Climate Change*, 5(1), 51–55. <https://doi.org/10.1038/nclimate2463>
- Livingstone, S. J., Utting, D. J., Ruffell, A., Clark, C. D., Pawley, S., Atkinson, N., & Fowler, A. C. (2016). Discovery of relict subglacial lakes and their geometry and mechanism of drainage. *Nature Communications*, 7(1), 1–9. <https://doi.org/10.1038/ncomms11767>
- Maier, N., Gimbert, F., & Gillet-Chaulet, F. (2022). Threshold response to melt drives large-scale bed weakening in Greenland. *Nature*, 607(7920), 714–720. <https://doi.org/10.1038/s41586-022-04927-3>
- Maier, N., Humphrey, N., Meierbachtol, T., & Harper, J. (2021). Deformation motion tracks sliding changes through summer, western Greenland. *Journal of Glaciology*, 68(267), 1–10. <https://doi.org/10.1017/jog.2021.87>
- Mejia, J., Gulley, J., Trunz, C., Covington, M., Bartholomew, T., Xie, S., & Dixon, T. (2021). Isolated cavities dominate Greenland ice sheet dynamic response to lake drainage. *Geophysical Research Letters*, 48(19), e2021GL094762. <https://doi.org/10.1029/2021gl094762>
- Morlighem, M. (2018). *IceBridge BedMachine Greenland, Version 3*. NASA National Snow and Ice Data Center Distributed Active Archive Center. <https://doi.org/10.5067/2CIX82HUV88Y>
- Morlighem, M., Williams, C. N., Rignot, E., An, L., Arndt, J. E., Bamber, J. L., et al. (2017). BedMachine v3: Complete bed topography and ocean bathymetry mapping of Greenland from multibeam echo sounding combined with mass conservation. *Geophysical Research Letters*, 44(21), 11–51. <https://doi.org/10.1002/2017gl074954>
- Mouginot, J., Rignot, E., Björk, A. A., Van Den Broeke, M., Millan, R., Morlighem, M., et al. (2019). Forty-six years of Greenland Ice Sheet mass balance from 1972 to 2018. *Proceedings of the National Academy of Sciences*, 116(19), 9239–9244. <https://doi.org/10.1073/pnas.1904242116>
- Podolskiy, E. A., Fujita, K., Sunako, S., & Sato, Y. (2019). Viscoelastic modeling of nocturnal thermal fracturing in a Himalayan debris-covered glacier. *Journal of Geophysical Research: Earth Surface*, 124(6), 1485–1515. <https://doi.org/10.1029/2018jg004848>
- Rada, C., & Schoof, C. (2018). Channelized, distributed, and disconnected: Subglacial drainage under a valley glacier in the Yukon. *The Cryosphere*, 12(8), 2609–2636. <https://doi.org/10.5194/tc-12-2609-2018>
- Ryser, C., Lüthi, M. P., Andrews, L. C., Catania, G. A., Funk, M., Hawley, R., et al. (2014). Caterpillar-like ice motion in the ablation zone of the Greenland ice sheet. *Journal of Geophysical Research: Earth Surface*, 119(10), 2258–2271. <https://doi.org/10.1002/2013jg003067>
- Schoof, C. (2005). The effect of cavitation on glacier sliding. *Proceedings of the Royal Society A: Mathematical, Physical & Engineering Sciences*, 461(2055), 609–627. <https://doi.org/10.1098/rspa.2004.1350>
- Schröder, L., Neckel, N., Zindler, R., & Humbert, A. (2020). Perennial supraglacial lakes in Northeast Greenland observed by polarimetric SAR. *Remote Sensing*, 12(17), 2798. <https://doi.org/10.3390/rs12172798>
- Sole, A., Nienow, P., Bartholomew, I., Mair, D., Cowton, T., Tedstone, A., & King, M. A. (2013). Winter motion mediates dynamic response of the Greenland Ice Sheet to warmer summers. *Geophysical Research Letters*, 40(15), 3940–3944. <https://doi.org/10.1002/grl.50764>
- Solgaard, A., Kusk, A., Merryman Boncori, J. P., Dall, J., Mankoff, K. D., Ahlstrøm, A. P., et al. (2021). Greenland ice velocity maps from the PROMICE project. *Earth System Science Data*, 13(7), 3491–3512. <https://doi.org/10.5194/essd-13-3491-2021>
- Stevens, L. A., Behn, M. D., McGuire, J. J., Das, S. B., Joughin, I., Herring, T., et al. (2015). Greenland supraglacial lake drainages triggered by hydrologically induced basal slip. *Nature*, 522(7554), 73–76. <https://doi.org/10.1038/nature14480>
- Tedesco, M., Willis, I. C., Hoffman, M. J., Banwell, A. F., Alexander, P., & Arnold, N. S. (2013). Ice dynamic response to two modes of surface lake drainage on the Greenland ice sheet. *Environmental Research Letters*, 8(3), 034007. <https://doi.org/10.1088/1748-9326/8/3/034007>
- Tsai, V. C., & Rice, J. R. (2010). A model for turbulent hydraulic fracture and application to crack propagation at glacier beds. *Journal of Geophysical Research: Earth Surface*, 115(F3), F03007. <https://doi.org/10.1029/2009jg001474>
- Tsai, V. C., Smith, L. C., Gardner, A. S., & Seroussi, H. (2022). A unified model for transient subglacial water pressure and basal sliding. *Journal of Glaciology*, 68(268), 390–400. <https://doi.org/10.1017/jog.2021.103>
- Van de crux, B., MacFerrin, M., Machguth, H., Colgan, W. T., van As, D., Heilig, A., et al. (2019). Firn data compilation reveals widespread decrease of firn air content in western Greenland. *The Cryosphere*, 13(3), 845–859. <https://doi.org/10.5194/tc-13-845-2019>
- Van de Wal, R., Smeets, C., Boot, W., Stoffelen, M., Van Kampen, R., Doyle, S. H., et al. (2015). Self-regulation of ice flow varies across the ablation area in south-west Greenland. *The Cryosphere*, 9(2), 603–611. <https://doi.org/10.5194/tc-9-603-2015>